

## SIMPLE MCBR MODELS OF CHEMICAL EVOLUTION: AN APPLICATION TO THE THIN AND THE THICK DISK

R. Caimmi

*Dipartimento di Fisica e Astronomia, Università di Padova  
Vicolo Osservatorio 3/2, I-35122 Padova, Italy*

E-mail: *roberto.caimmi@unipd.it*

(Received: July 3, 2012; Accepted: November 1, 2012)

**SUMMARY:** Simple multistage closed-(box+reservoir) (MCBR) models of chemical evolution, formulated in an earlier attempt, are extended to the limit of dominant gas inflow or outflow with respect to gas locked up into long-lived stars and remnants. For an assigned empirical differential oxygen abundance distribution (EDOD), which can be linearly fitted, a family of theoretical differential oxygen abundance distribution (TDOD) curves is built up with the following prescriptions: (i) the initial and the ending points of the linear fit are common to all curves; (ii) the flow parameter  $\kappa$  ranges from an extremum point to  $\mp\infty$ , where negative and positive  $\kappa$  correspond to inflow and outflow, respectively; (iii) the cut parameter  $\zeta_O$  ranges from an extremum point (which cannot be negative) to the limit  $(\zeta_O)_\infty$  related to  $|\kappa| \rightarrow +\infty$ . For curves with increasing  $\zeta_O$ , the gas mass fraction locked up into long-lived stars and remnants is found to attain a maximum and then decrease towards zero as  $|\kappa| \rightarrow +\infty$  while the remaining parameters show a monotonic trend. The theoretical integral oxygen abundance distribution (TIOD) is also expressed. An application is made to the EDOD deduced from two different samples of disk stars, for both the thin and the thick disk. The constraints on formation and evolution are discussed in the light of the model. The evolution is tentatively subdivided into four stages, namely: assembling (A), formation (F), contraction (C), equilibrium (E). The EDOD related to any stage is fitted by all curves where  $0 \leq \zeta_O \leq (\zeta_O)_\infty$  for inflowing gas and  $(\zeta_O)_\infty \leq \zeta_O \leq 1.2$  for outflowing gas, with a single exception related to the thin disk (A stage), where the range of fitting curves is restricted to  $0.35 \leq \zeta_O \leq (\zeta_O)_\infty$ . The F stage may safely be described by a steady inflow regime ( $\kappa = -1$ ), implying a flat TDOD, in agreement with the results of hydrodynamical simulations. Finally, (1) the change of fractional mass due to the extension of the linear fit to the EDOD, towards both the (undetected) low-metallicity and high-metallicity tail, is evaluated and (2) the idea of a thick disk - thin disk collapse is discussed, in the light of the model.

Key words. galaxies: evolution - stars: formation – stars: evolution

### 1. INTRODUCTION

The empirical metallicity distributions of long-lived stars belonging to different populations

constrain models for the formation and the evolution of the Galaxy. Simple multistage closed-(box+reservoir) (MCBR) models formulated in an earlier attempt (Caimmi 2011a, hereafter quoted as

C11) make a useful tool in the description of Galactic chemical evolution. In particular, MCBR models allow for gas inflow or outflow with specified metal abundance ratio with respect to the pre existing gas, but general conclusions can also be inferred (C11). The special case of steady inflow regime, where the infalling gas exactly balances the net amount of gas turned into stars, finds a counterpart in the results of hydrodynamical simulations, where a quasi equilibrium is attained between the inflowing gas, outflowing gas and gas lost via star formation (e.g. Finlator and Davé 2008, Davé et al. 2011a,b, 2012).

For different populations within the Galaxy, the empirical differential oxygen abundance distribution (EDOD) shows the existence of three different regimes of chemical evolution, where gas inflow is initially the dominant process, followed by a nearly steady inflow regime, while gas outflow prevails at later times (C11 and references therein). Understanding of different stages of Galactic (or sub Galactic) chemical evolution can be used to get further insight in the evolution of important global properties of stellar and gaseous component of galaxies.

The current paper is aimed to (i) extension and improvement of MCBR models and (ii) their application to the thin and the thick disk. The extension of the model is concerned with the limit of dominant inflowing or outflowing gas rate in comparison to star formation rate and calculation of related quantities which, for assigned input values, restricts the parameter space. In addition, the theoretical integral oxygen abundance distribution (TIOD) is explicitly expressed. The improvement of the model consists in a different choice of the family of fitting theoretical differential oxygen abundance distribution (TDOD) curves with respect to an earlier attempt (C11), which can be used for any kind of environment.

With regard to an assigned stage of evolution, the starting and the ending points of the linear fit to the EDOD are in common to each curve of the family, instead of the intercept and the ending point as in the parent paper (C11). The difference is negligible if the model is applied to populations with initial oxygen abundance close to zero such as the halo (C11), while it is considerable for populations with initial oxygen abundance substantially larger than zero, such as the thin and the thick disk, which are dealt with in the current paper.

The EDOD for the thin and the thick disk is inferred from two different samples in Section 2. Extension and improvement of MCBR models is presented in Section 3. An application to the thin and the thick disk is shown in Section 4. The results are discussed in Section 5. The conclusion is drawn in Section 6.

## 2. THE EDOD FOR THE THIN AND THE THICK DISK

### 2.1. General remarks

The abundance distribution of a generic nuclide Q for star samples, is binned in  $[Q/H]=$

$\log(n_Q/n_H) - \log(n_Q/n_H)_\odot$ , where  $n_Q, n_H$ , are number abundances. On the other hand, the comparison between the empirical differential metal abundance distribution and its theoretical counterpart predicted by a model implies the knowledge of the normalized mass abundance,  $\phi_Q = Z_Q/(Z_Q)_\odot$ . It can be seen that  $\log \phi_Q = [Q/H]$  to a good extent. For further details refer to an earlier attempt (Caimmi 2007).

In terms of mass abundance, the bin centre and the bin semiamplitude read:

$$\phi_Q = \frac{1}{2} \{ \exp_{10} [Q/H]^+ + \exp_{10} [Q/H]^- \} ; \quad (1)$$

$$\Delta^\mp \phi_Q = \frac{1}{2} \{ \exp_{10} [Q/H]^+ - \exp_{10} [Q/H]^- \} ; \quad (2)$$

which implies a variable bin width in  $\phi_Q$  for a constant bin width in  $[Q/H]$ .

The differential metal abundance distribution has been dealt with in earlier attempts in both non normalized (Pagel 1989, Malinie et al. 1993) and normalized (Rocha-Pinto and Maciel 1996, Caimmi 2000, 2001a,b, 2007) form, the latter one to be used in the following. The related bin centre and the bin semiamplitude read:

$$\psi_Q = \log \frac{\Delta N}{N \Delta \phi_Q} ; \quad (3)$$

$$\Delta^\mp \psi_Q = \log \left[ 1 \mp \frac{(\Delta N)^{1/2}}{\Delta N} \right] ; \quad (4)$$

where  $\Delta N$  is the number of sample stars within the metal abundance bin,  $\Delta \phi_Q = \Delta^- \phi_Q + \Delta^+ \phi_Q$  centered on  $\phi_Q$ ,  $N$  is the total number of sample stars, and the uncertainty on  $\Delta N$  has been evaluated from Poissonian errors as  $\sigma_{\Delta N} = (\Delta N)^{1/2}$  (e.g. Ryan and Norris 1991). It is worth noticing that the semiamplitudes,  $\Delta^\mp \psi_Q$ , are different and, in particular,  $\Delta^- \psi_Q \rightarrow -\infty$  for  $\Delta N = 1$ , which implies caution has to be used with bins containing a single star. For further details refer to earlier attempts (Caimmi 2001b, 2007).

From this point on, attention will be restricted only to oxygen, Q=O, where  $\phi_O = \phi$  and  $\psi_O = \psi$  will be used to simplify the notation. On the other hand, the results of the current paper hold for any primary element which is synthesized mainly within type II supernova progenitors.

### 2.2. The data

Oxygen abundance determination in stellar atmospheres is intrinsically difficult, so that different methods yield different results (e.g. Ramirez et al. 2007, Fabbian et al. 2009) and no general consensus as yet exists. For this reason, the population of available samples does not exceed a few hundredths at most. For further details refer to earlier attempts (Caimmi 2007, 2008, Caimmi and Milanese 2009, C11).

As for the disk, the data will be inferred from samples studied in earlier attempts (Ramirez et al. 2007, Petigura and Marcy 2011), where oxygen abundance has been determined both in presence and in absence of the local thermodynamical approximation (LTE) in the former case and only in presence of LTE in the latter. The samples extracted from the above mentioned parent papers are listed in Table 1.

**Table 1.** Samples used for determining the empirical differential oxygen abundance distribution (EDOD) of the thin and the thick disk. Sample denomination relates to the parent sample (Ra07 - Ramirez et al. 2007, PM11 - Petigura and Marcy 2011) and to the population [k - thick disk (TK); n - thin disk (TN); stars uncertain if TK or TN are denoted as UN]. Presence or absence of the LTE approximation for oxygen abundance determination is denoted as yes or no, respectively. The total number of sample stars is  $N$ .

| sample | population | $N$     | LTE |
|--------|------------|---------|-----|
| Ra07k  | TK         | 133     | no  |
| Ra07n  | TN         | 310     | no  |
| PM11k  | TK + UN    | 14 + 20 | yes |
| PM11n  | TN         | 624     | yes |

With regard to Ra07 samples, the EDOD has been inferred in an earlier attempt (Caimmi and Milanese 2009) both in presence and in absence of the

LTE approximation and only the latter case will be considered in the current investigation.

The EDOD inferred from PM11 samples is presented in Table 2.

### 2.3. Linear fit to the EDOD

Both Ra07 and PM11 samples are biased towards low metallicities,  $[\text{Fe}/\text{H}] \lesssim -1$  which, using the  $[\text{O}/\text{H}]-[\text{Fe}/\text{H}]$  relation inferred in the parent paper (Ramirez et al. 2007), translates into  $\phi \lesssim 0.3$  for both the thin and the thick disk. On the other hand, thin disk stars exhibit oxygen abundance above 0.3 within both Ra07n (Caimmi and Milanese 2009) and PM11n (Table 2) samples, while both Ra07k (Caimmi and Milanese 2009) and PM11k (Table 2) samples show a low-metallicity tail below 0.3.

It may safely be assumed that the low-metallicity tail relates to a negligible mass fraction for the thin and (to a lesser extent) for thick disk. Accordingly, sufficiently large samples listed in Table 1 (PM11n, Ra07n, Ra07k) can be considered as representative for the thin or the thick disk, while the remaining small sample (PM11k) is added for comparison only.

For all samples listed in Table 1, the EDOD is plotted in Fig. 1, where upper and lower panels represent PM11 and Ra07 samples, respectively.

Points with lower error bars reaching the horizontal axis (including the one out of scale) correspond to bins containing a single star.

**Table 2.** The empirical differential oxygen abundance distribution (EDOD) in the thin and thick disk, deduced from the PM11 sample ( $N = 658$ ). The error on the generic bin height has been estimated from the Poissonian error. Disk stars belonging to uncertain population ( $N = 20$ ) have been included within thick disk stars ( $N = 14$ ) to get larger population ( $N = 34$ ). The bin width in  $[\text{O}/\text{H}] = \log \phi$  is  $\mp 0.05$ . Label captions: TN - thin disk; TK - thick disk; UN - uncertain whether belonging to thin or thick disk. See text for further details.

| $\phi$    | TN         |        | TK + UN    |     | $\Delta N$ |    |
|-----------|------------|--------|------------|-----|------------|----|
|           | $\psi$     | $\psi$ | $\psi$     | TN  | TK         | UN |
| 1.2673D-1 |            |        | +5.3464D-3 | 0   | 1          | 0  |
| 1.5954D-1 |            |        |            | 0   | 0          | 0  |
| 2.0085D-1 |            |        |            | 0   | 0          | 0  |
| 2.5286D-1 |            |        |            | 0   | 0          | 0  |
| 3.1833D-1 |            |        |            | 0   | 0          | 0  |
| 4.0075D-1 | -1.4573D-0 |        | -4.9465D-1 | 2   | 1          | 0  |
| 5.0451D-1 | -1.0802D-0 |        | -2.9362D-1 | 6   | 1          | 1  |
| 6.3514D-1 | -4.9596D-1 |        | -3.9362D-1 | 29  | 1          | 1  |
| 7.9960D-1 | -3.7170D-2 |        | -1.9259D-1 | 105 | 2          | 2  |
| 1.0066D-0 | -1.8480D-2 |        | -2.9259D-1 | 138 | 1          | 3  |
| 1.2673D-0 | -7.9393D-3 |        | -9.1564D-2 | 178 | 2          | 6  |
| 1.5954D-0 | -2.7200D-1 |        | -1.9156D-1 | 122 | 5          | 3  |
| 2.0085D-0 | -8.5630D-1 |        | -7.1753D-1 | 40  | 0          | 3  |
| 2.5286D-0 | -1.9563D-0 |        | -1.2947D-0 | 4   | 0          | 1  |

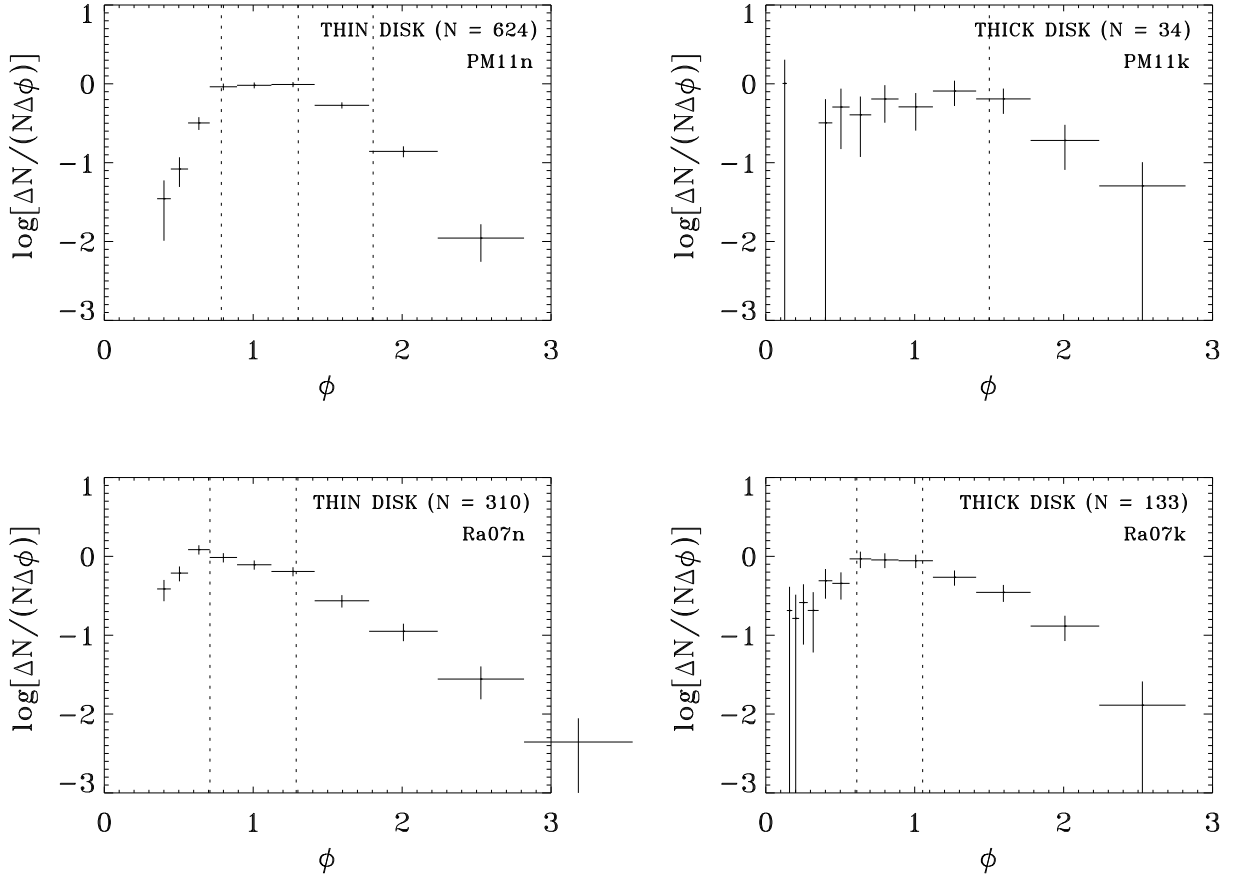


**Fig. 1.** The empirical differential oxygen abundance distribution (EDOD) related to PM11 (upper panels) and Ra07 (lower panels) samples. The uncertainty of the distribution is determined from Poisson errors, which tend to negative infinite for data related to a single star, including the one outside the bottom left panel. The vertical dotted lines mark the boundary between adjacent regions, as determined from the intersection of related linear fits. For further details refer to the text.

The main feature of the EDOD, plotted in Fig. 1, is the presence of up to four regions exhibiting a nearly linear trend, which will be labelled A, F, C, E, for increasing oxygen abundance. Linear fits to each region,  $\psi = a\phi + b$ , are performed using the bisector regression (Caimmi 2011b), leaving aside bins related to single stars, unless the total number of points reduces to two. Aiming to a unified description, the number of regions will be kept equal to four in all cases and adjacent regions with coinciding linear trend will be indicated by related letters e.g. CE means regions C and E are fitted by the same line. The regression line slope and intercept esti-

matoms and related dispersion estimators are listed in Table 3 for each region of the EDOD plotted in Fig. 1.

The regression lines are represented in Fig. 2 for each region, according to slope and intercept values listed in Table 3. To ensure continuity, adjacent regions are bounded by the intersections of related regression lines.

The results are listed in Table 4 where O denotes oxygen abundance ranges without data,  $0 \leq \phi \leq \phi_i$  and  $\phi \geq \phi_f$ , where  $\phi_i$  and  $\phi_f$  are the minimum and maximum oxygen abundance, respectively, within sample stars.

**Table 3.** Regression line slopes and intercept estimators,  $\hat{a}$  and  $\hat{b}$ , and related dispersion estimators,  $\hat{\sigma}_{\hat{a}}$  and  $\hat{\sigma}_{\hat{b}}$ , for bisector regression models applied to the oxygen abundance distribution (EDOD) plotted in different panels of Fig. 1. The method requires dealing with each region (X) separately. Data points on the boundary between adjacent regions are used for determining regression lines within both of them.

| X  | $\hat{a}$   | $\hat{\sigma}_{\hat{a}}$ | $\hat{b}$   | $\hat{\sigma}_{\hat{b}}$ | sample |
|----|-------------|--------------------------|-------------|--------------------------|--------|
| A  | +3.6420 E+0 | 1.4136 E-1               | -2.8981 E+0 | 6.6652 E-2               | PM11n  |
| F  | +6.3321 E-2 | 5.7541 E-3               | -8.6073 E-2 | 5.8764 E-3               |        |
| C  | -1.1689 E+0 | 7.0570 E-2               | +1.5193 E+0 | 1.2997 E-1               |        |
| E  | -1.8294 E+0 | 8.0990 E-2               | +2.7116 E+0 | 1.8562 E-1               |        |
| A  | +2.1371 E+0 | 3.9906 E-2               | -1.2771 E+0 | 2.2528 E-2               | Ra07n  |
| F  | -4.3676 E-1 | 3.0185 E-2               | +3.4846 E-1 | 2.8952 E-2               |        |
| CE | -1.0703 E+0 | 1.3474 E-2               | +1.1649 E+0 | 2.2887 E-2               |        |
| AF | +2.7877 E-1 | 7.8677 E-2               | -5.1247 E-1 | 7.1999 E-2               | PM11k  |
| CE | -1.1799 E+0 | 1.8906 E-2               | +1.6773 E+0 | 4.1322 E-2               |        |
| A  | +1.8383 E+0 | 2.4630 E-1               | -1.1545 E+0 | 1.3187 E-1               | Ra07k  |
| F  | -6.4249 E-2 | 2.8011 E-3               | +8.2504 E-3 | 2.3791 E-3               |        |
| CE | -8.1530 E-1 | 3.4051 E-2               | +7.8279 E-1 | 4.4835 E-2               |        |

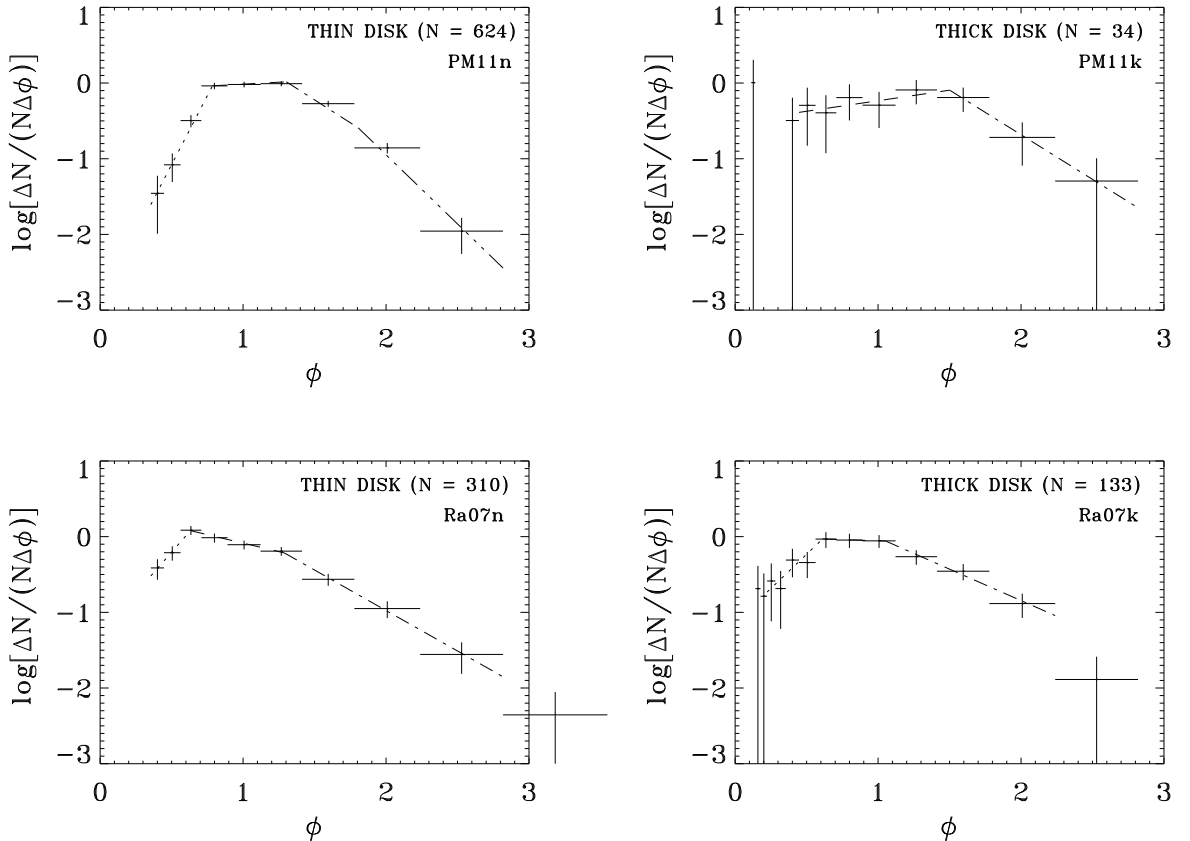


**Fig. 2.** Regression lines for the empirical differential oxygen abundance distribution (EDOD) plotted in Fig. 1, with regard to the regions (from the left to the right): A, F, C, E. If adjacent regions exhibit a similar linear trend, a single fit is performed. Data related to a single star are not used for the fitting procedure unless only two points remain. Other captions as in Fig. 1.

**Table 4.** Transition points between adjacent regions, as determined from the intersection of related regression lines, for the oxygen abundance distribution (EDOD) plotted in different panels of Fig. 1. The repetition of the data passing from a one stage to the next means that the interpolation line remains unchanged and any point may be considered as a transition point. Cases on the left and on the right relate to thin and thick disk, respectively (left and right panels of Fig. 1). Cases at the top and at the bottom relate to PM11 and Ra07 samples, respectively (top and bottom panels of Fig. 1).

| sample<br>transition | PM11n / Ra07n |             | PM11k / Ra07k |             |
|----------------------|---------------|-------------|---------------|-------------|
|                      | $\phi$        | $\psi$      | $\phi$        | $\psi$      |
| O-A                  | 4.0075 E-1    | -1.4386 E+0 | 5.0451 E-1    | -3.7183 E-1 |
| A-F                  | 7.8579 E-1    | -3.6316 E-2 | 5.0451 E-1    | -3.7183 E-1 |
| F-C                  | 1.3028 E+0    | -3.5782 E-3 | 1.5012 E-0    | -9.3977 E-2 |
| C-E                  | 1.8052 E+0    | -5.9085 E-1 | 1.5012 E-0    | -9.3977 E-2 |
| E-O                  | 2.5286 E+0    | -1.9141 E-0 | 2.5286 E-0    | -1.3061 E-0 |
| O-A                  | 4.0075 E-1    | -4.2062 E-1 | 2.5286 E-1    | -6.8969 E-1 |
| A-F                  | 6.3155 E-1    | +7.2630 E-2 | 6.1116 E-1    | -3.1016 E-2 |
| F-C                  | 1.2887 E-0    | -2.1439 E-1 | 1.0313 E-0    | -5.8008 E-2 |
| C-E                  | 1.2887 E-0    | -2.1439 E-1 | 1.0313 E-0    | -5.8008 E-2 |
| E-O                  | 2.5286 E-0    | -1.5414 E-0 | 2.0085 E-0    | -8.5474 E-1 |

Accordingly, a vertical line instead of a regression line is considered for the intersection points related to O-A and E-O transitions.

In conclusion, the EDOD related to the thin and the thick disk may be conceived, to a satisfactory extent, as due to the contribution of four (A, F, C, E) or three (A, F, CE) or two (AF, CE) regions within which the trend is linear. An interpolation in terms of MCBR models of chemical evolution is highly attractive in that the corresponding TDOD shows, as a special case, a linear trend (C11).

### 3. THE MODEL

#### 3.1. General remarks

Simple MCBR models have been presented in an earlier paper (C11) and an interested reader is addressed therein for an exhaustive formulation. Only what is relevant for the application will be repeated here and related extension and improvement will be performed. The main assumptions of the model are listed below.

- System structured as a box and a reservoir where gas can be exchanged between the two but mass conservation holds.
- Instantaneous recycling within the box, where stars are divided into two categories, namely (a) short-lived which instantaneously evolve, and (b) long-lived all of which are still evolving.
- Instantaneous mixing within the box.
- Gas outflow from the box into the reservoir or inflow into the box from the reservoir at a rate proportional to the star formation rate and with fixed composition.
- Inhibition of star formation within the reservoir.

- Oxygen abundance proportional to metal abundance according to the forthcoming Eq. (8).

In this picture, the gas mass fraction  $\mu$  (normalized to the initial mass) and the oxygen abundance  $\phi$  (normalized to the solar value) are related as:

$$\frac{\mu}{\mu_i} = \left[ \frac{1 - c\phi}{1 - c\phi_i} \right]^{(Z_O)_\odot / (c\hat{p}'')} ; \quad (5)$$

$$c = \frac{(Z_O)_\odot}{\hat{p}} [A_O \hat{p} - \kappa(1 - \zeta_O)] ; \quad (6)$$

$$\hat{p}'' = \frac{\hat{p}}{1 + \kappa} ; \quad (7)$$

$$Z = A_O Z_O ; \quad (8)$$

where  $(Z_O)_\odot$  is the solar oxygen abundance,  $\hat{p}$  is the yield,  $\hat{p}''$  the effective yield,  $\kappa$  the flow (positive for outflow and negative for inflow),  $\zeta_O$  the cut,  $Z_O$  the oxygen abundance,  $Z$  the metal abundance,  $A_O = 2$  to an acceptable extent and the index  $i$  denotes values at the beginning of evolution.

More specifically,  $\kappa$  represents the ratio of gas mass locked into long-lived stars and stellar remnants to gas mass outflowed into the reservoir or inflowed from the reservoir and  $\zeta_O$  represents the ratio of oxygen abundance within the flowing gas to oxygen abundance within the pre existing gas. For further details refer to the parent paper (C11). In principle,  $-\infty < \kappa < +\infty$  and  $0 \leq \zeta_O \leq A_O / (Z_O)_f$ . The domain  $\zeta_O > A_O / (Z_O)_f$  is in contradiction with the assumption of fixed  $\zeta_O$  during the evolution.

The TDOD predicted by the model reads:

$$\psi = \left[ \frac{(Z_O)_\odot}{c\hat{p}''} - 1 \right] \log(1 - c\phi) + b ; \quad (9)$$

$$b = \log \left[ \frac{\mu_i}{\mu_i - \mu_f} \frac{(Z_O)_\odot}{\hat{p}''} \right] - \frac{(Z_O)_\odot}{c\hat{p}''} \log(1 - c\phi_i); \quad (10)$$

where  $b$  is the intercept of the curve on the  $(O\phi\psi)$  plane. For further details refer to the parent paper (C11).

### 3.2. Theoretical integral oxygen abundance distribution (TIOD)

An explicit expression of the TIOD could be needed for a number of applications. The theoretical counterpart of the EDOD, via Eq. (3), reads:

$$\psi = \log \frac{dN}{(N_f - N_i) d\phi} ; \quad (11)$$

where  $N_i$ ,  $N_f$ , denote the total number of long-lived stars with normalized oxygen abundance,  $\phi \leq \phi_i$ ,  $\phi \leq \phi_f$ , respectively.

The combination of Eqs. (9) and (11) after some algebra yields:

$$\frac{dN}{N_f - N_i} = 10^b (1 - c\phi)^{(Z_O)_\odot / (c\hat{p}'') - 1} d\phi ; \quad (12)$$

which can be integrated. The result is:

$$\frac{N - N_i}{N_f - N_i} = -10^b \frac{\hat{p}''}{(Z_O)_\odot} \left[ (1 - c\phi)^{(Z_O)_\odot / (c\hat{p}'')} - (1 - c\phi_i)^{(Z_O)_\odot / (c\hat{p}'')} \right] ; \quad (13)$$

where  $N$  is the total number of stars with normalized oxygen abundance not exceeding  $\phi$ . Accordingly, the TIOD is expressed by Eq. (13).

### 3.3. A family of TDOD curves

The TDOD, expressed by Eq. (9), via (5), (6), (7), (10), depends on the input parameters  $[A_O, \hat{p}, (Z_O)_\odot, \phi_i, \phi_f, \mu_i]$  and the output parameters  $(\kappa, \zeta_O)$ . With regard to a selected stage of evolution (or adjacent stages fitted by the same line), let  $(\phi_i, \psi_i)$  and  $(\phi_f, \psi_f)$  be the starting and the ending points, respectively, of the related linear fit. The family of TDOD curves passing through the above mentioned points necessarily satisfy the relations:

$$\psi_i = \left[ \frac{(Z_O)_\odot}{c\hat{p}''} - 1 \right] \log(1 - c\phi_i) + b ; \quad (14)$$

$$\psi_f = \left[ \frac{(Z_O)_\odot}{c\hat{p}''} - 1 \right] \log(1 - c\phi_f) + b ; \quad (15)$$

which makes a system of two equations in the two unknowns  $(\kappa, \zeta_O)$ .

The combination of Eqs. (14) and (15) after some algebra yields:

$$\kappa = \frac{c\hat{p}}{(Z_O)_\odot} \left[ 1 + (\psi_f - \psi_i) \left( \log \frac{1 - c\phi_f}{1 - c\phi_i} \right)^{-1} - 1 \right] ; \quad (16)$$

which, for assigned  $\zeta_O$ , can be solved by repeated iterations using Eq. (6) until  $|\kappa^{(n)} - \kappa^{(n-1)}| < \epsilon$ , where  $n$  is the last iteration and  $\epsilon$  a fixed threshold. Then the generic curve of the family is defined by the parameters,  $(\kappa, \zeta_O)$ . The intercept  $b$  is determined via Eq. (14) or (15).

Both the EDOD and the TDOD can be represented on the  $(O\phi\psi)$  plane, the former and the latter normalized to the long-lived star population of the sample and the environment under consideration, respectively, which translates into a normalization constant  $\log C_N$ . More specifically, the TDOD has to be vertically shifted on the  $(O\phi\psi)$  plane by a value  $\log C_N$  to match the EDOD. The result is:

$$C_N = 10^b \frac{\hat{p}''}{(Z_O)_\odot} \frac{\mu_i - \mu_f}{\mu_i} (1 - c\phi_i)^{(Z_O)_\odot / (c\hat{p}'')} ; \quad (17)$$

where  $b$  is defined by Eq. (10). For further details refer to the parent paper (C11) keeping in mind that the family of TDOD curves defined therein have in common the points  $(0, b)$  and  $(\phi_f, \psi_f)$  instead of  $(\phi_i, \psi_i)$  and  $(\phi_f, \psi_f)$ , respectively.

### 3.4. The linear limit

In the special case  $c = 0$ , Eq. (6) reduces to:

$$\zeta_O = 1 - \frac{A_O \hat{p}}{\kappa} ; \quad (18)$$

which implies  $\zeta_O > 1$  for  $\kappa < 0$ ;  $0 \leq \zeta_O < 1$  for  $\kappa \geq A_O \hat{p}$ ;  $\zeta_O = 1$  for  $|\kappa| \rightarrow +\infty$ ;  $\zeta_O < 0$  for  $0 \leq \kappa < A_O \hat{p}$ . The last subdomain has to be excluded as negative cut values, by definition, have no physical meaning.

With regard to the remaining domain Eqs. (5), (9), (10), (13), reduce to:

$$\frac{\mu}{\mu_i} = \exp \left[ -\frac{(Z_O)_\odot}{\hat{p}''} (\phi - \phi_i) \right] ; \quad (19)$$

$$\psi = a\phi + b ; \quad (20)$$

$$b = \log \left[ \frac{\mu_i}{\mu_i - \mu_f} (-\ln 10) a \right] - a\phi_i ; \quad (21)$$

$$a = -\frac{1}{\ln 10} \frac{(Z_O)_\odot}{\hat{p}''} ; \quad (22)$$

$$\frac{N - N_i}{N_f - N_i} = \frac{1}{\ln 10} \frac{1}{a} [\exp_{10}(a\phi + b) - \exp_{10}(a\phi_i + b)] ; \quad (23)$$

implying a linear TDOD on the  $(O\phi\psi)$  plane. Accordingly, the limit  $c \rightarrow 0$ , will be referred to as the linear limit.

Keeping in mind that the starting and the ending points of the linear fit are  $(\phi_i, \psi_i)$  and  $(\phi_f, \psi_f)$  respectively, an empirical counterpart of Eq. (20) reads:

$$\psi = \psi_i + \frac{\psi_f - \psi_i}{\phi_f - \phi_i}(\phi - \phi_i) ; \quad (24)$$

which implies, by comparison with Eq. (20) via (7) and (22):

$$a = \frac{\psi_f - \psi_i}{\phi_f - \phi_i} = a_0(1 + \kappa) ; \quad (25)$$

$$a_0 = -\frac{1}{\ln 10} \frac{(Z_O)_\odot}{\hat{p}} ; \quad (26)$$

where  $a_0$  is the slope related to stagnation regime,  $\kappa = 0$ . Accordingly,  $\kappa = a/a_0 - 1$  and Eq. (18) takes the form:

$$\zeta_O = 1 + \frac{A_O \hat{p}}{1 - a/a_0} ; \quad (27)$$

where the output parameters  $(\kappa, \zeta_O)$  may be determined using Eqs. (25)-(27).

### 3.5. The dominant flow limit

In the limit of negligible star formation rate with respect to flow rate,  $|\kappa| \rightarrow +\infty$ , the following relations hold:

$$\lim_{|\kappa| \rightarrow +\infty} \left[ \frac{(Z_O)_\odot}{c\hat{p}''} \right] = -\frac{1}{1 - \zeta_O} ; \quad (28)$$

$$\lim_{|\kappa| \rightarrow +\infty} \left[ \frac{(Z_O)_\odot}{\hat{p}''} \frac{1}{1 - c\phi_i} \right] = \frac{1}{1 - \zeta_O} \frac{1}{\phi_i} ; \quad (29)$$

$$\lim_{|\kappa| \rightarrow +\infty} \left[ \log \frac{1 - c\phi}{1 - c\phi_i} \right] = \log \frac{\phi}{\phi_i} ; \quad (30)$$

$$\begin{aligned} \lim_{|\kappa| \rightarrow +\infty} \left\{ b + \left[ \frac{(Z_O)_\odot}{c\hat{p}''} - 1 \right] \log(1 - c\phi_i) \right\} \\ = \log \left[ \frac{\mu_i}{\mu_i - \mu_f} \frac{1}{1 - \zeta_O} \frac{1}{\phi_i} \right] ; \end{aligned} \quad (31)$$

and Eqs. (5) and (9) reduce to:

$$\lim_{|\kappa| \rightarrow +\infty} \frac{\mu}{\mu_i} = \left( \frac{\phi}{\phi_i} \right)^{-1/(1-\zeta_O)} ; \quad (32)$$

$$\begin{aligned} \lim_{|\kappa| \rightarrow +\infty} \psi = \frac{\zeta_O - 2}{1 - \zeta_O} \log \frac{\phi}{\phi_i} \\ + \log \left[ \frac{\mu_i}{\mu_i - \mu_f} \frac{1}{1 - \zeta_O} \frac{1}{\phi_i} \right] ; \end{aligned} \quad (33)$$

where the last relation implies a divergence for the intercept,  $\psi(0) \rightarrow \infty$ .

The particularization of Eq. (33) to the points  $(\phi_i, \psi_i)$  and  $(\phi_f, \psi_f)$ , yields:

$$\psi_f - \psi_i = \frac{\zeta_O - 2}{1 - \zeta_O} \log \frac{\phi_f}{\phi_i} ; \quad (34)$$

accordingly, the cut,  $\zeta_O$ , after some algebra reads:

$$\zeta_O = \frac{(\psi_f - \psi_i) + 2 \log(\phi_f/\phi_i)}{(\psi_f - \psi_i) + \log(\phi_f/\phi_i)} = \frac{a/\gamma + 2}{a/\gamma + 1} ; \quad (35)$$

$$\gamma = \frac{\log(\phi_f/\phi_i)}{\phi_f - \phi_i} ; \quad (36)$$

where  $a$  is the slope of the linear fit expressed by Eq. (25) and  $\gamma > 0$ .

The intercept  $b$  according to Eq. (31), can be expressed as:

$$b = b' - \left[ \frac{(Z_O)_\odot}{c\hat{p}''} - 1 \right] \log(1 - c\phi_i) ; \quad (37)$$

$$b' = \log \left[ \frac{\mu_i}{\mu_i - \mu_f} \frac{1}{1 - \zeta_O} \frac{1}{\phi_i} \right] ; \quad (38)$$

where  $\kappa \rightarrow \mp\infty$  necessarily implies  $\mu_i \stackrel{<}{>} \mu_f$  and, in turn,  $\zeta_O \stackrel{>}{<} 1$ , within the domain of the reduced intercept  $b'$  expressed by Eq. (38). Keeping in mind Eq. (6), the last term on the right-hand side of Eq. (37) in the case under discussion shows a divergence as:

$$\begin{aligned} \lim_{|\kappa| \rightarrow +\infty} \left\{ \left[ \frac{(Z_O)_\odot}{c\hat{p}''} - 1 \right] \log(1 - c\phi_i) \right\} \\ = \frac{\zeta_O - 2}{1 - \zeta_O} \lim_{|\kappa| \rightarrow +\infty} \log(1 - c\phi_i) = \infty ; \end{aligned} \quad (39)$$

accordingly, the normalization constant  $C_N$  must be related to the reduced intercept  $b'$  whose empirical counterpart equals  $\psi_i$ , via Eqs. (14) and (37). Then Eq. (17) translates into:

$$C_N = 10^{\psi_i} \frac{\mu_i - \mu_f}{\mu_i} (1 - \zeta_O) \phi_i ; \quad (40)$$

which is equivalent to  $\psi_i = b' + \log C_N$ .

### 3.6. The $(O\kappa\zeta_O)$ plane

The linear limit  $c = 0$  is represented on the  $(O\kappa\zeta_O)$  plane via Eq. (18) as an equilateral hyperbola of asymptotes  $\kappa = 0$  and  $\zeta_O = 1$  shown in Fig. 3.

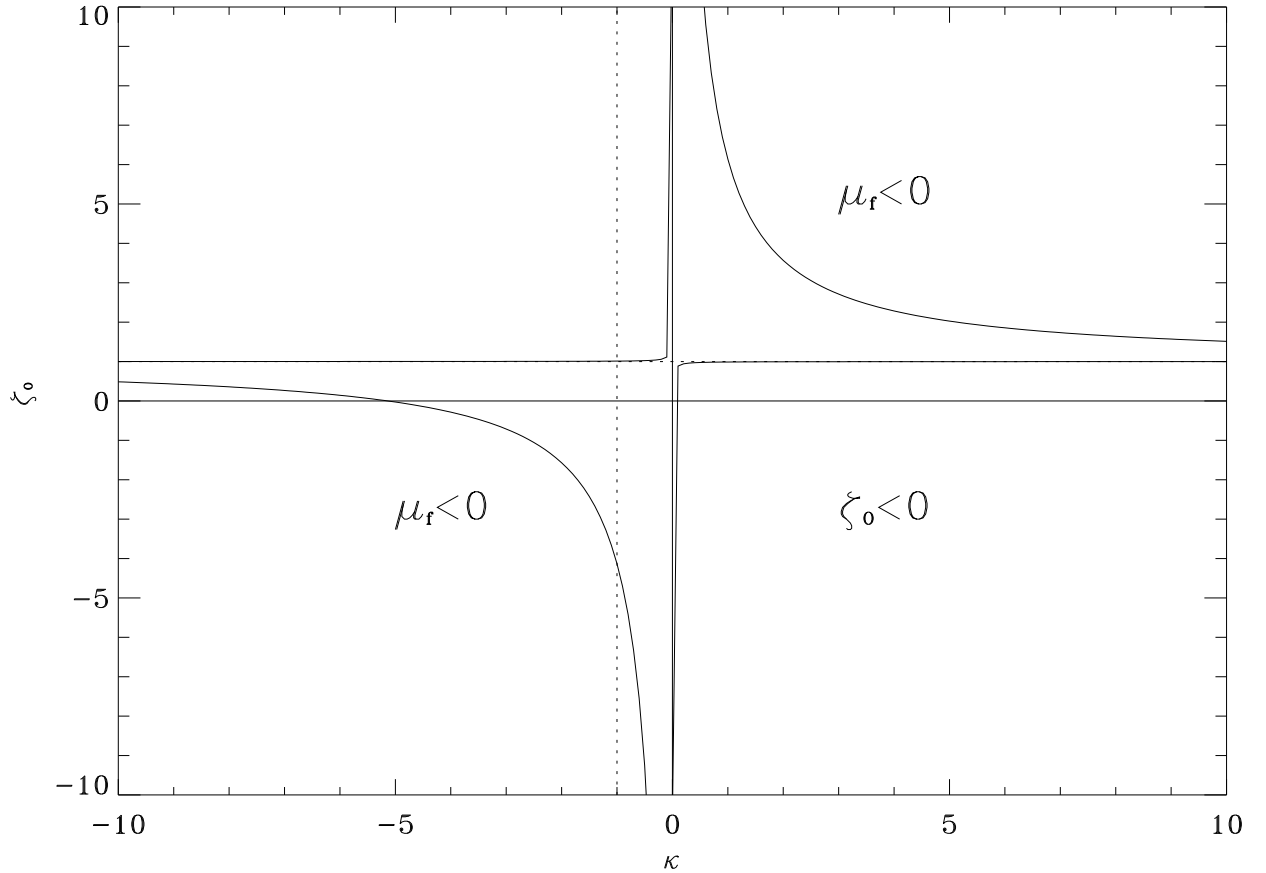


**Fig. 3.** The parameter space on the  $(O\kappa\zeta_O)$  plane. The locus  $c = 0$  is represented by the equilateral hyperbola lying in the second and fourth quadrant, where  $c > 0$  or  $c < 0$  for points placed between the branches of the hyperbola or outside either branch, respectively. The locus  $\mu_f = 0$  is represented by the equilateral hyperbola lying in the first and third quadrant, where  $\mu_f > 0$  or  $\mu_f < 0$  for points placed between the branches of the hyperbola or outside either branch, respectively. The vertical axis  $\kappa = 0$  and the horizontal axis  $\zeta_O = 1$  are asymptotes for both hyperbolas. The vertical axis  $\kappa = -1$  represents the steady inflow regime. The parameter space is restricted to the region bounded by the branches of the hyperbola  $\mu_f = 0$  and the horizontal axis  $\zeta_O = 0$  which ensures  $\mu_f \geq 0$  and  $\zeta_O \geq 0$ .

It can be seen that  $c > 0$  for points lying between the branches of the hyperbola, while  $c < 0$  for points lying outside either branch of the hyperbola.

The steady inflow regime  $\kappa = -1$  is represented in the  $(O\kappa\zeta_O)$  plane as a vertical axis. It can be seen that  $\mu_f > \mu_i$  in the strong inflow regime,  $\kappa < -1$  and  $\mu_f < \mu_i$  in the weak inflow regime  $-1 < \kappa < 0$  either in the stagnation regime  $\kappa = 0$  or in outflow regime  $\kappa > 0$  while  $\mu_f = \mu_i$  in the steady inflow regime.

The limit of complete gas exhaustion via Eq. (5) reads  $c = 1/\phi_f$ , which, using Eq. (6), can be cast into the explicit form:

$$\zeta_O = 1 - \left[ A_O \hat{p} - \frac{\hat{p}}{(Z_O)_\odot} \frac{1}{\phi_f} \right] \frac{1}{\kappa} ; \quad (41)$$

that is an equilateral hyperbola with asymptotes  $\kappa = 0$ ,  $\zeta_O = 1$  as shown in Fig. 3. It can be seen that  $\mu_f > 0$  for points lying between the branches of the hyperbola, while  $\mu_f < 0$  for points lying outside either branch of the hyperbola. The latter implies lack of physical meaning, together with points lying on the negative semiplane  $\zeta_O < 0$ . Accordingly, the parameter space on the  $(O\kappa\zeta_O)$  plane is restricted to the region bounded by the branches of the hyperbola expressed by Eq. (41) and the horizontal axis  $\zeta_O = 0$  where  $\mu_f \geq 0$ ,  $\zeta_O \geq 0$ , as shown in Fig. 3.

It is worth noticing that  $c\phi_f \rightarrow 1$  implies  $|\psi(\phi_f)| \rightarrow +\infty$  via Eq. (9), and the related curve cannot belong to the family defined by Eqs. (14) and (15).

#### 4. RESULTS

The EDOD corresponding to the samples considered in Section 2 can be divided into four, three, or two regions, where the trend is linear to a good extent, as shown in Fig. 2. In the light of the model, each region corresponds to a different stage of chemical evolution, which can tentatively be related to a different stage of dynamical evolution. For further details refer to the parent paper (C11).

The fractional mass of the box (with respect to the initial value) attains the maximum value at the end of the last stage P where the TDOD still shows a slope  $a > a_0$  i.e. inflow regime (into the box from the reservoir). The related value is  $(\mu_P)_f + (s_P)_f$ . The fractional stellar mass of the box at the end of evolution, which coincides with the end of the last stage L is  $(s_L)_f$ . Accordingly, the mass ratio of the box at the end of evolution to the outflowed gas reads:

$$\frac{M_{\text{box}}}{M_{\text{off}}} = \frac{(\mu_L)_f + (s_L)_f}{(\mu_P)_f + (s_P)_f - (\mu_L)_f - (s_L)_f} ; \quad (42)$$

provided earlier stages with respect to P are in inflow regime and later stages in outflow regime.

Following the procedure outlined in the parent paper (C11) and keeping the same values of the input parameters,  $(Z_O)_\odot = 0.0056$ ,  $\hat{p}/(Z_O)_\odot = 1.0340$ ,  $\mu_i = 1$ ,  $s_i = 0$ ;  $D_i = 0$ , the normalization constant, the cut, the flow, the active gas mass fraction, the star mass fraction, and the inflowed or outflowed gas mass fraction at the end of each stage of evolution can be computed. The results are listed in Tables 5 and 6 where different cases are related to different EDOD data plotted in Fig. 1. The index U denotes

a stage (or adjacent stages) of evolution where the trend is linear to a good extent and the indices lin and  $\infty$  mark the linear and the dominant flow limit, respectively.

**Table 5.** Output parameters  $[(\zeta_O)_U]_{\text{lin}}$  and  $[(\zeta_O)_U]_{\infty}$  related to the linear limit (lin) and to the dominant flow limit ( $\infty$ ) for simple MCBR models where the theoretical differential oxygen abundance distribution (TDOD) provides a linear fit to the empirical differential oxygen abundance distribution (EDOD) plotted in different panels of Fig. 1. Four, three, or two stages of evolution are considered, according to the linear trends exhibited by the EDOD.

| U  | $[(\zeta_O)_U]_{\text{lin}}$ | $[(\zeta_O)_U]_{\infty}$ | sample |
|----|------------------------------|--------------------------|--------|
| A  | 1.0012E+0                    | 1.1726E+0                | PM11n  |
| F  | 1.0101E+0                    | 1.8702E+0                |        |
| C  | 9.9351E-1                    | 6.8213E-1                |        |
| E  | 9.9655E-1                    | 8.7566E-1                |        |
| A  | 1.0019E+0                    | 1.2860E+0                | Ra07n  |
| F  | 7.0971E-1                    | 1.4628E+1                |        |
| CE | 9.9252E-1                    | 7.1698E-1                |        |
| AF | 1.0070E+0                    | 1.6302E+0                | PM11k  |
| CE | 9.9360E-1                    | 7.7029E-1                |        |
| A  | 1.0023E+0                    | 1.3778E+0                | Ra07k  |
| F  | 1.0138E+0                    | 2.1469E+0                |        |
| CE | 9.8770E-1                    | 4.2840E-1                |        |

**Table 6.** Output parameters  $(C_U)_N$ ,  $\kappa_U$ ,  $(\mu_U)_f$ ,  $(s_U)_f$  and  $(D_U)_f$  for simple MCBR models where the theoretical differential oxygen abundance distribution (TDOD) provides a linear fit to the empirical differential oxygen abundance distribution (EDOD) plotted in different panels of Fig. 1. Other captions as in Table 5.

| U  | $(C_U)_N$ | $\kappa_U$ | $(\mu_U)_f$ | $(s_U)_f$ | $(D_U)_f$  | sample |
|----|-----------|------------|-------------|-----------|------------|--------|
| A  | 1.0534E-1 | -9.6714E+0 | 2.5253E+1   | 2.7969E+0 | -2.7050E+1 | PM11n  |
| F  | 4.9391E-1 | -1.1508E+0 | 2.7230E+1   | 1.5911E+1 | -4.2141E+1 |        |
| C  | 2.7317E-1 | +1.7831E+0 | 7.0432E+0   | 2.3164E+1 | -2.9207E+1 |        |
| E  | 5.8008E-2 | +3.3557E+0 | 3.3456E-1   | 2.4704E+1 | -2.4039E+1 |        |
| A  | 1.6306E-1 | -6.0883E+0 | 3.1135E+0   | 4.1536E-1 | -2.5289E+0 | Ra07n  |
| F  | 5.6841E-1 | +3.9895E-2 | 1.6078E+0   | 1.8633E+0 | -2.4711E+0 |        |
| CE | 2.3602E-1 | +1.5483E+0 | 7.5727E-2   | 2.4645E+0 | -1.5402E+0 |        |
| AF | 5.9299E-1 | -1.6637E+0 | 1.8961E+0   | 1.3500E+0 | -2.2461E+0 | PM11k  |
| CE | 8.7126E-1 | +1.8093E+0 | 1.1633E-1   | 1.9835E+0 | -1.0999E+0 |        |
| A  | 1.7169E-1 | -5.3769E+0 | 4.5570E+0   | 8.1266E-1 | -4.3696E+0 | Ra07k  |
| F  | 5.5095E-1 | -8.4703E-1 | 4.2824E+0   | 2.6077E+0 | -5.8901E+0 |        |
| CE | 9.4260E-1 | +9.4119E-1 | 6.8384E-1   | 4.4615E+0 | -4.1454E+0 |        |

The mass ratio of the box at the end of evolution to the outflowed gas, expressed by Eq. (42), and the box mass fraction at the end of evolution,  $(M_{\text{box}})_f / (M_{\text{box}})_i = (\mu_L)_f + (s_L)_f$ , can be inferred from Table 6 where  $P = F, A, AF$ , and  $L = E, CE$ , according to the case. The result is (leaving aside the poorly populated PM11k sample)  $M_{\text{box}}/M_{\text{off}} = 1.4$ - $2.6$  for the thin disk and  $2.9$  for the thick disk;  $(M_{\text{box}})_f / (M_{\text{box}})_i = 2.5$ - $25.0$  for the thin disk and  $5.6$  for the thick disk.

The validity of the linear limit implies cut values very close to unity,  $\zeta_{\text{O}} \approx 1$ , unless  $\kappa \rightarrow 0^-$  or  $\kappa \rightarrow (A_{\text{O}}\hat{p})^+$  according to Eq. (18), as can be seen in Table 6. On the other hand, inflowing gas from the intergalactic medium is expected to be oxygen-poor with respect to galaxies, while outflowing gas into

galactic medium is expected to be slightly oxygen-rich with respect to pre existing gas. For this reason, the departure from the linear limit must also be considered.

The results are shown in Fig. 4 where, in addition to the linear limit shown in Fig. 2, the following cases are also represented:  $\zeta_{\text{O}} = 0, (\zeta_{\text{O}})_{\infty}$ , for  $\kappa < 0$  i.e. the inflow regime, and  $\zeta_{\text{O}} = (\zeta_{\text{O}})_{\infty}, 1.2$ , for  $\kappa > 0$  i.e. the outflow regime. In general, curves from up to down correspond to decreasing cut  $\zeta_{\text{O}}$ . All curves remain close to the related linear limit and fit to the data with the exception of the A stage corresponding to the PM11n sample where curves within the range  $0 \leq \zeta_{\text{O}} < 0.35$  do not match the whole set of error boxes. The curve related to  $\zeta_{\text{O}} = 0.35$  is also plotted on the top left panel of Fig. 4.

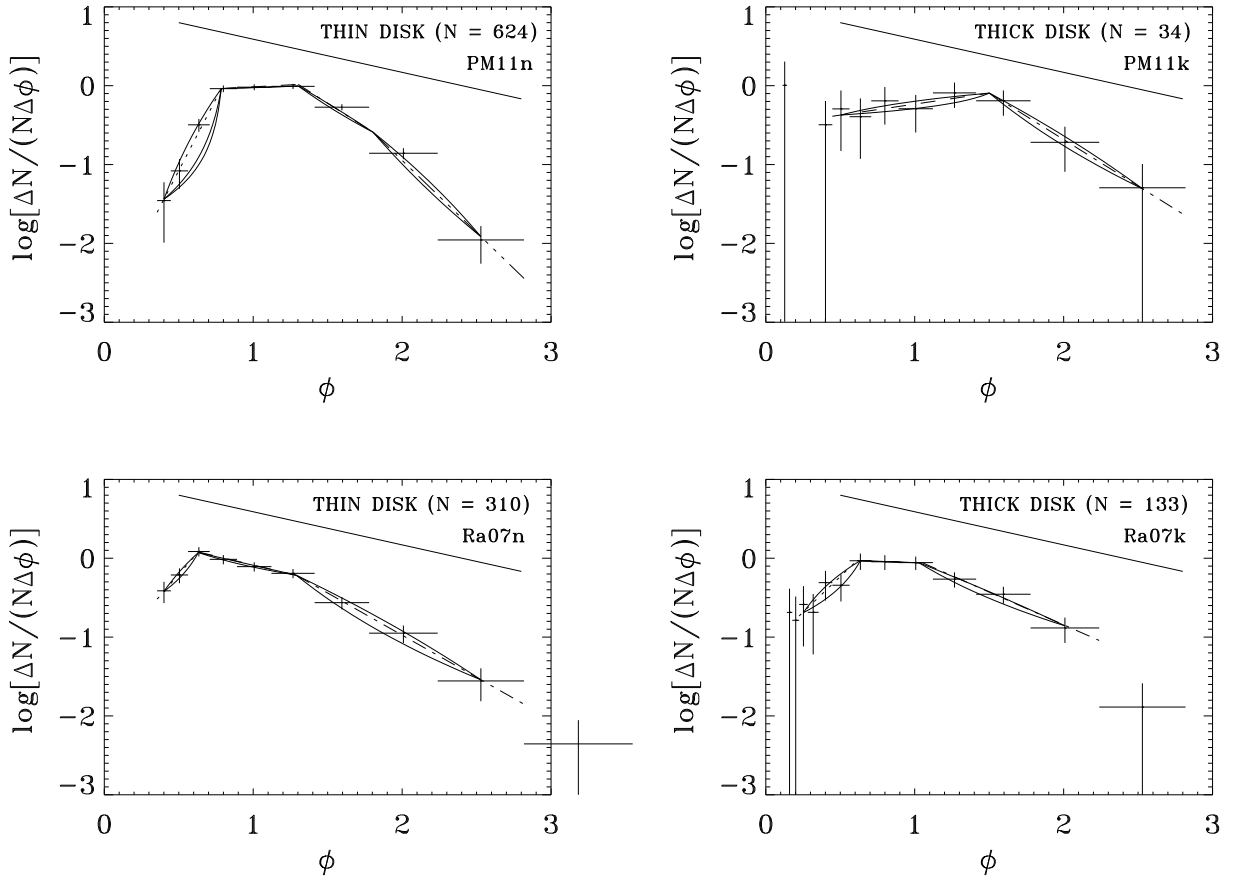


**Fig. 4.** Comparison between empirical (EDOD) plotted in Fig. 1 and theoretical (TDOD) differential oxygen abundance distribution defined by the family of curves including the regression line and passing through the starting point  $(\phi_i, \psi_i)$  and the ending point  $(\phi_f, \psi_f)$  where  $\psi_u = a\phi_u + b_N$ ,  $u = i, f$ ,  $b_N = b + \log C_N$ , for the stage under consideration. Curves correspond (from bottom to top) to cut values  $\zeta_{\text{O}}$  between 0 and  $(\zeta_{\text{O}})_{\infty}$ , or  $(\zeta_{\text{O}})_{\infty}$  and 1.2 for negative and positive flow values  $\kappa$ , respectively. With regard to the top left panel, the lower curve fitting the data corresponds to  $\zeta_{\text{O}} = 0.35$ . In general, for varying cut,  $(\zeta_{\text{O}})_{\text{min}} \leq \zeta_{\text{O}} \leq (\zeta_{\text{O}})_{\text{max}}$ , the TDOD lies within the region bounded by the curves  $\zeta_{\text{O}} = (\zeta_{\text{O}})_{\text{min}}$  and  $\zeta_{\text{O}} = (\zeta_{\text{O}})_{\text{max}}$ . The full straight line on the top of each panel has slope  $a_0 = -(1/\ln 10)[(Z_{\text{O}})_{\text{O}}/\hat{p}] = -0.42$  and relates to null flow  $\kappa = 0$ , thus separating the inflow regime  $a > a_0$ ,  $\kappa < 0$  from the outflow regime  $a < a_0$ ,  $\kappa > 0$ . A horizontal straight line corresponds to the steady inflow regime  $a = 0$ ,  $\kappa = -1$ .

**Table 7.** Values of the cut  $\zeta_{\text{O}}$ , the flow  $\kappa$ , the fractional active gas mass  $\mu_f$ , the fractional long-lived star mass  $s_f$ , the fractional flowing gas mass  $D_f$ , the parameter  $c$ , and the normalization constant  $C_{\text{N}}$  for the family of theoretical differential oxygen abundance distributions which contains the curves plotted in Fig. 4, top left panel, restricted to A stage. In addition,  $\zeta_{\text{lin}} = 1.0012$  and  $\zeta_{\infty} = 1.1726$  as listed in Table 5.

| $\zeta_{\text{O}}$   | $-\kappa$ | $\mu_f$   | $s_f$     | $-D_f$    | $c$        | $C_{\text{N}}$ |
|----------------------|-----------|-----------|-----------|-----------|------------|----------------|
| 0.00                 | 1.2587E+0 | 1.7268E+0 | 2.8099E+0 | 3.5367E+0 | +1.2284E+0 | 5.3730E-2      |
| 0.10                 | 1.3860E+0 | 2.1334E+0 | 2.9360E+0 | 4.0694E+0 | +1.2176E+0 | 5.6624E-2      |
| 0.20                 | 1.5407E+0 | 2.6596E+0 | 3.0693E+0 | 4.7290E+0 | +1.2032E+0 | 5.9859E-2      |
| 0.30                 | 1.7323E+0 | 3.3487E+0 | 3.2072E+0 | 5.5560E+0 | +1.1839E+0 | 6.3482E-2      |
| 0.35                 | 1.8462E+0 | 3.7728E+0 | 3.2765E+0 | 6.0493E+0 | +1.1718E+0 | 6.5455E-2      |
| 0.40                 | 1.9754E+0 | 4.2627E+0 | 3.3450E+0 | 6.6077E+0 | +1.1574E+0 | 6.7546E-2      |
| 0.50                 | 2.2932E+0 | 5.4925E+0 | 3.4740E+0 | 7.9665E+0 | +1.1201E+0 | 7.2111E-2      |
| 0.60                 | 2.7752E+0 | 7.1749E+0 | 3.5792E+0 | 9.7541E+0 | +1.0654E+0 | 7.7246E-2      |
| 0.65                 | 3.0047E+0 | 8.2475E+0 | 3.6152E+0 | 1.0863E+1 | +1.0282E+0 | 8.0052E-2      |
| 0.70                 | 3.3446E+0 | 9.5204E+0 | 3.6341E+0 | 1.2154E+1 | +9.8155E-1 | 8.3030E-2      |
| 0.75                 | 3.7663E+0 | 1.1040E+1 | 3.6292E+0 | 1.3669E+1 | +9.2179E-1 | 8.6193E-2      |
| 0.80                 | 4.3029E+0 | 1.2839E+1 | 3.5919E+0 | 1.5456E+1 | +8.4346E-1 | 8.9553E-2      |
| 0.90                 | 5.9747E+0 | 1.7756E+1 | 3.3683E+0 | 2.0125E+1 | +5.8900E-1 | 9.6916E-2      |
| 1.00                 | 9.6022E+0 | 2.5143E+1 | 2.8067E+0 | 2.6950E+1 | +1.1200E-2 | 1.0523E-1      |
| $\zeta_{\text{lin}}$ | 9.6714E+0 | 2.5253E+1 | 2.7969E+0 | 2.7050E+1 | 0          | 1.0534E-1      |
| 1.10                 | 2.3278E+1 | 3.6730E+1 | 1.6039E+0 | 3.7334E+1 | -2.2400E+0 | 1.1463E-1      |
| 1.15                 | 7.5661E+1 | 4.5018E+1 | 5.8956E-1 | 4.4607E+1 | -1.0964E+1 | 1.1977E-1      |
| 1.16                 | 1.3622E+2 | 4.6946E+1 | 3.3979E-1 | 4.6286E+1 | -2.1067E+1 | 1.2084E-1      |
| 1.17                 | 6.7115E+2 | 4.8979E+1 | 7.1595E-2 | 4.8051E+1 | -1.1033E+2 | 1.2192E-1      |
| $\zeta_{\infty}$     | $+\infty$ | 4.9516E+1 | 0         | 4.8516E+1 | $-\infty$  | 1.2219E-1      |

As for the PM11n sample restricted to the A stage, values of parameters which characterize the family of TDOD curves considered in Subsection 3.2, are listed in Table 7.

The linear limit, the dominant flow limit, together with other curves plotted in Fig. 4, top left panel, A stage, are also included. Due to the occurrence of inflow regime, the flow  $\kappa$  and related fractional flowing mass  $D$  are negative by definition. All the parameters listed in Table 7 exhibit a monotonic trend with the exception of the long-lived star fractional mass  $s_f$ , which attains a maximum at  $\zeta_{\text{O}} \approx 0.70$  and decreases to zero in the dominant flow limit  $\zeta_{\text{O}} = (\zeta_{\text{O}})_{\infty}$ . In particular, the TDOD fits to the EDOD within the range  $0.35 \lesssim \zeta_{\text{O}} \leq (\zeta_{\text{O}})_{\infty}$  related to  $-1.85 \gtrsim \kappa > -\infty$ ,  $3.77 \lesssim \mu_f \lesssim 49.52$ ,  $0 \leq s_f \lesssim 3.63$ . It can also be seen that the normalization constant  $C_{\text{N}}$  is changed only slightly with respect to the linear limit  $\zeta_{\text{O}} = (\zeta_{\text{O}})_{\text{lin}}$ .

In the general case of a varying oxygen abundance within the flowing gas, i.e. varying cut  $(\zeta_{\text{O}})_{\text{min}} \leq \zeta_{\text{O}} \leq (\zeta_{\text{O}})_{\text{max}}$  the TDOD belonging

to the family of curves passing through the points  $(\phi_i, \psi_i)$ ,  $(\phi_f, \psi_f)$  intersects all curves characterized by constant  $\zeta_{\text{O}}$  in the range under consideration, lying within the region bounded by the curves where  $\zeta_{\text{O}} = (\zeta_{\text{O}})_{\text{min}}$  and  $\zeta_{\text{O}} = (\zeta_{\text{O}})_{\text{max}}$ . As shown in Fig. 4, the TDOD fits to the EDOD over the whole range of  $\zeta_{\text{O}}$  with the restriction  $(\zeta_{\text{O}})_{\text{min}} = 0.35$  for the A stage, top left panel (middle full curve).

Values of the active gas, long-lived star and flowing gas mass fraction at the end of each stage are listed in Table 8. for the linear limit (upper rows) and the lowest curve fitting to the data (lower rows) which corresponds to  $(\zeta_{\text{O}})_{\text{min}} = 0.35$  for the PM11n sample, and  $(\zeta_{\text{O}})_{\text{min}} = 0$  for Ra07n, PM11k, Ra07k samples, with regard to the initial A stage.

The linear limit is assumed during the following F, C and E stage. An inspection of Table 8. discloses that the active gas mass fraction is lowered by a factor up to about 7, while long-lived star and flowing gas mass fraction are lowered by a factor up to about 4, passing from the linear limit  $\zeta_{\text{O}} = (\zeta_{\text{O}})_{\text{lin}}$  to the lowest curve fitting to the data  $\zeta_{\text{O}} = (\zeta_{\text{O}})_{\text{min}}$  at the end of evolution.

**Table 8.** Values of active gas, long-lived star and flowing gas mass fractions at the end of each stage for the extreme situations of inflowing gas during the earlier stage (A) with oxygen abundance equal to  $\zeta_{\text{O}} = (\zeta_{\text{O}})_{\text{lin}}$  (upper rows) and  $\zeta_{\text{O}} = (\zeta_{\text{O}})_{\text{min}}$  (lower rows) with respect to pre existing gas, in connection with the thin (top cases) and thick (bottom cases) disk. The values of the cut related to lower curves still consistent with the data, plotted in Fig. 4, are  $(\zeta_{\text{O}})_{\text{min}} = 0.35$  (PM11n sample), 0 (Ra07n, PM11k, Ra07k samples). During the subsequent F, C, and E stage,  $\zeta_{\text{O}} = (\zeta_{\text{O}})_{\text{lin}}$  has been assumed.

| U  | $(\mu_{\text{U}})_f$ | $(s_{\text{U}})_f$ | $(D_{\text{U}})_f$ | sample |
|----|----------------------|--------------------|--------------------|--------|
| A  | 2.5253E+1            | 2.7969E+0          | -2.7050E+1         | PM11n  |
|    | 3.7728E+0            | 3.2765E+0          | -6.0493E+0         |        |
| F  | 2.7230E+1            | 1.5911E+1          | -4.2141E+1         |        |
|    | 4.0681E+0            | 5.2358E+0          | -8.3039E+0         |        |
| C  | 7.0432E+0            | 2.3164E+1          | -2.9207E+1         |        |
|    | 1.0523E+0            | 6.3194E+0          | -6.3717E+0         |        |
| E  | 3.3456E-1            | 2.4704E+1          | -2.4039E+1         |        |
|    | 4.9984E-2            | 6.5495E+0          | -5.5995E+0         |        |
| A  | 3.1135E-0            | 4.1536E-1          | -2.5289E-0         | Ra07n  |
|    | 1.2393E-0            | 7.7920E-1          | -1.0185E-0         |        |
| F  | 1.6078E-0            | 1.8633E-0          | -2.4711E-0         |        |
|    | 6.3995E-1            | 1.3555E-0          | -9.9548E-1         |        |
| CE | 7.5727E-2            | 2.4645E-0          | -1.5402E-0         |        |
|    | 3.0142E-2            | 1.5948E-0          | -6.2497E-1         |        |
| AC | 1.8961E-0            | 1.3500E-0          | -2.2461E-0         | PM11k  |
|    | 3.0081E-1            | 1.7505E-0          | -1.0513E-0         |        |
| CE | 1.1633E-1            | 1.9835E-0          | -1.0999E-0         |        |
|    | 1.8456E-2            | 1.8510E-0          | -8.6944E-1         |        |
| A  | 4.5570E-0            | 8.1266E-1          | -4.3696E-0         | Ra07k  |
|    | 1.3223E-0            | 1.0925E-0          | -1.4148E-0         |        |
| F  | 4.2824E-0            | 2.6077E-0          | -5.8901E-0         |        |
|    | 1.2474E-0            | 1.5537E-0          | -1.8011E-0         |        |
| CE | 6.8384E-1            | 4.4615E-0          | -4.1454E-0         |        |
|    | 1.9836E-1            | 2.0941E-0          | -1.2925E-0         |        |

## 5. DISCUSSION

As shown in Fig. 2, the EDOD inferred from PM11 and Ra07 samples for the thin and the thick disk (see Table 1) can be fitted by a straight line on four, three or two adjacent regions. In the light of simple MCBR models of chemical evolution, the TDOD is represented by a family of curves (including the straight line) passing through the starting and the ending points  $(\phi_i, \psi_i)$  and  $(\phi_f, \psi_f)$ , respectively, of a selected stage of evolution. Accordingly, different stages of evolution relate to different linear fits to the EDOD where an initial strong inflow regime ( $a > 0$ ) is followed by a steady ( $a = 0$ ) or moderate ( $-0.42 < a < 0$ ) inflow regime and finally by a stagnation ( $a = -0.42$ ) or outflow ( $a < -0.42$ ) regime. For further details refer to an earlier paper (C11).

The above description is in agreement with the results of hydrodynamical simulations where quasi

equilibrium is attained between inflowing gas, outflowing gas and gas lost via star formation after an early stage of strong inflow and, presumably, before a late stage of strong outflow (e.g. Finlator and Davé 2008, Davé et al. 2011a,b, 2012). Within the formalism of simple MCBR models, both the inflow and the outflow rate are proportional to the star formation rate and, for this reason, only the net effect  $\kappa = \kappa_{\text{in}} + \kappa_{\text{out}}$ ,  $\zeta_{\text{O}} = (\zeta_{\text{O}})_{\text{in}} + (\zeta_{\text{O}})_{\text{out}}$  is considered.

Though the assumption of null stellar mass fraction holds to an acceptable extent for the starting configuration, the presence of stars with oxygen abundance lower than in sample objects,  $\phi < 0.4$  or  $[\text{O}/\text{H}] < -0.4$  for the thin disk, and  $\phi < 0.2$  or  $[\text{O}/\text{H}] < -0.7$  for the thick disk, has still to be considered. To this aim, samples unbiased towards low oxygen abundance (not available at present) should be used.

The thick disk is expected to be affected from this inconvenience to a larger extent with respect to the thin disk due to a more extended low-metallicity

tail. In any case, the results of the current paper may be thought of as representative of the chemical evolution of the thin disk for  $\phi \geq 0.4$  or  $[\text{O}/\text{H}] \geq -0.4$ , and of the thick disk for  $\phi \geq 0.3$  or  $[\text{O}/\text{H}] \geq -0.5$ , the latter being related to  $[\text{Fe}/\text{H}] \geq -1$  where the data are unbiased (Ramirez et al. 2007, Petigura and Marcy 2011).

As shown in Fig.4, the TDOD fits to the EDOD regardless of the value of the cut,  $\zeta_{\text{O}}$ , i.e. the oxygen abundance ratio of flowing to pre existing gas, within a plausible range where the physical meaning of the problem is preserved. The sole exception relates to the PM11n sample (Fig. 4, top left), A stage, where curves within the range  $0 \leq \zeta_{\text{O}} < 0.35$  provide a poor fit to the data, which implies inflow of low-metallicity gas within the thin disk, could not take place when the pre existing gas was sufficiently oxygen-enriched,  $[\text{O}/\text{H}] \gtrsim -0.4$ .

The above result can be extended to the case of variable cut  $(\zeta_{\text{O}})_{\text{min}} \leq \zeta_{\text{O}} \leq (\zeta_{\text{O}})_{\text{max}}$  where the TDOD lies between the region bounded by the curves related to  $(\zeta_{\text{O}})_{\text{min}}$  and  $(\zeta_{\text{O}})_{\text{max}}$ , respectively. Then the differential distribution of oxygen abundance in thin disk and thick disk stars (leaving aside the low-metallicity tail) depends only slightly on the oxygen abundance of the flowing gas.

Biases towards low-metallicity and high-metallicity stars may be corrected under the assumption that the TDODs related to  $\phi < \phi_i$  and  $\phi > \phi_f$ , respectively, allow analytical continuation. Let  $\phi_{\text{min}}$  and  $\phi_{\text{max}}$  be the unknown initial and final normalized oxygen abundances related to stages A and E, respectively.

The fractional number of long-lived stars with normalized oxygen abundance  $\phi_{\text{min}} \leq \phi \leq \phi_i$  can be inferred from Eq. (13) as:

$$\frac{(\delta N)_{\text{A}}}{N_f - N_i} = -10^{b_{\text{A}}} \frac{\hat{p}''}{(Z_{\text{O}})_{\odot}} \left[ (1 - c_{\text{A}}\phi_i)^{(Z_{\text{O}})_{\odot}/(c_{\text{A}}\hat{p}'')} - (1 - c_{\text{A}}\phi_{\text{min}})^{(Z_{\text{O}})_{\odot}/(c_{\text{A}}\hat{p}'')} \right] ; \quad (43)$$

or, in the linear limit ( $c \rightarrow 0$ ), from Eq. (23), as:

$$\frac{(\delta N)_{\text{A}}}{N_f - N_i} = \frac{1}{\ln 10} \frac{1}{a_{\text{A}}} \left[ \exp_{10}(a_{\text{A}}\phi_i + b_{\text{A}}) - \exp_{10}(a_{\text{A}}\phi_{\text{min}} + b_{\text{A}}) \right] ; \quad (44)$$

where, in any case, the maximum value relates to  $\phi_{\text{min}} = 0$ .

The fractional number of long-lived stars with normalized oxygen abundance  $\phi_f \leq \phi \leq \phi_{\text{max}}$  can be inferred from Eq. (13) as:

$$\frac{(\delta N)_{\text{E}}}{N_f - N_i} = -10^{b_{\text{E}}} \frac{\hat{p}''}{(Z_{\text{O}})_{\odot}} \left[ (1 - c_{\text{E}}\phi_{\text{max}})^{(Z_{\text{O}})_{\odot}/(c_{\text{E}}\hat{p}'')} - (1 - c_{\text{E}}\phi_f)^{(Z_{\text{O}})_{\odot}/(c_{\text{E}}\hat{p}'')} \right] ; \quad (45)$$

or, in the linear limit ( $c \rightarrow 0$ ), from Eq. (23), as:

$$\frac{(\delta N)_{\text{E}}}{N_f - N_i} = \frac{1}{\ln 10} \frac{1}{a_{\text{E}}} \left[ \exp_{10}(a_{\text{E}}\phi_{\text{max}} + b_{\text{E}}) - \exp_{10}(a_{\text{E}}\phi_f + b_{\text{E}}) \right] ; \quad (46)$$

where, in any case, the maximum value relates to  $\phi_{\text{max}} = A_{\text{O}}/(Z_{\text{O}})_{\odot}$  via Eq. (8) which implies  $Z = 1$  and may be replaced, with unrelevant numerical change in the results, by  $\phi_{\text{max}} \rightarrow +\infty$ .

Due to the presence of (undetected) low-metallicity and high-metallicity tail in the EDOD, the fractional star mass change at the end of evolution, can be inferred under the assumption that star number is proportional to star mass,  $\delta N/N = \delta s_f/s_f$ . The result is:

$$\frac{\delta s_f}{s_f} = \frac{(\delta N)_{\text{A}} + (\delta N)_{\text{E}}}{N_f - N_i} ; \quad (47)$$

where the values of the parameters can be deduced from the linear fits to the EDOD as shown in Tables 3 and 4. The results are listed in Table 9, with regard to upper values, in the linear limit.

**Table 9.** Upper values of the fractional star mass change due to the low-metallicity tail (A), the high-metallicity tail (E), both tails (A+E), under the assumption that the linear fit to the EDOD remains unchanged outside the oxygen abundance range covered by the parent sample. Calculations were performed in the linear limit using values listed in Tables 3 and 4 together with  $\phi_{\text{min}} = 0$  and  $\phi_{\text{max}} = A_{\text{O}}/(Z_{\text{O}})_{\odot}$  i.e.  $Z = 1$  which, for practical purposes, is equivalent to  $\phi_{\text{max}} \rightarrow +\infty$ .

| $(\delta s_f)_{\text{A}}/s_f$ | $(\delta s_f)_{\text{E}}/s_f$ | $(\delta s_f)_{\text{A+E}}/s_f$ | sample |
|-------------------------------|-------------------------------|---------------------------------|--------|
| 4.1925 E-3                    | 2.8929 E-3                    | 7.0854 E-3                      | PM11n  |
| 6.6414 E-2                    | 1.1666 E-2                    | 7.8079 E-2                      | Ra07n  |
| 1.8307 E-1                    | 1.8189 E-2                    | 2.0126 E-1                      | PM11k  |
| 3.1718 E-2                    | 7.4427 E-2                    | 1.0614 E-1                      | Ra07k  |

It can be seen that the larger contribution arises from the low-metallicity tail for PM11k sample and from the high-metallicity tail for Ra07k sample. The reason is that, in both cases, the paucity of data makes metallicity tails more extended, as shown in Fig. 2. The total change in fractional star mass does not exceed about 10% at most with the exception of the (poorly populated) PM11k sample where it raises to about 20%. Accordingly, the results of the current paper hold to an acceptable extent even if the linear trend shown by the EDOD is extended to undetected metallicity tails.

In general, the disk is usually conceived as made of two main subsystems: the thick disk and the thin disk. Accordingly, the EDOD related to the disk depends on the thick to thin disk mass ratio  $M_{\text{K}}/M_{\text{N}}$  which is poorly known at present. Values quoted in the literature span a wide range from some percent (e.g. Holmberg et al. 2007) to about unity

(e.g. Fuhrmann 2008) or even indeterminate in the sense that no distinction can be made (e.g. Norris 1987, Ivezić et al. 2008, Bovy et al. 2012). Very low values of  $M_K/M_N$  could be biased unless corrected taking into consideration the different heights of the two subsystems above the Galactic plane at the Sun.

The idea of a thick disk - thin disk collapse is not in contradiction with related specific angular momentum distribution as shown in earlier works (Wyse and Gilmore 1992, Ibata and Gilmore 1995). If this is the case, in the light of the model, the thick and thin disk gas and star fractional mass are normalized to the same initial mass and the mass ratio of the thick to the thin disk at the end of evolution reads:

$$\frac{M_K}{M_N} = \frac{(s_f)_K}{(\mu_f)_K + (\mu_f)_N + (s_f)_N} ; \quad (48)$$

where  $s_f$  and  $\mu_f$  correspond to the end of evolution and the indices K and N denote the thick and the thin disk, respectively. From the results given in Table 6, it can be inferred  $M_K/M_N = 0.08, 1.89$ , for PM11 and Ra07 samples, respectively. The former value would argue for a thick disk - thin disk collapse, but the PM11k sample is poorly populated to draw firm conclusions. On the other hand, the latter value would be against a thick disk - thin disk collapse unless a massive thick disk (with respect to the thin disk) is recognized. Finally, if a single (thick + thin) disk population exists, the EDOD stays close to its counterpart inferred both from the PM11n sample, due to the smallness of the PM11k sample, and from the Ra07n sample, as shown in an earlier attempt (Caimmi and Milanese 2009).

The family of TDOD curves, considered for each stage of evolution, is characterized by two common points  $(\phi_i, \psi_i)$  and  $(\phi_f, \psi_f)$  which make the boundary of the related linear fit. As shown in Table 7 for the PM11n sample, A stage, curves with increasing cut  $\zeta_O$  exhibit a monotonic trend for the remaining parameters with the exception of the star mass fraction at the end of evolution  $s_f$  which attains a maximum. Accordingly, for a selected stage of evolution and fixed starting and ending points of the related linear fit to the EDOD, the star formation efficiency cannot exceed a threshold. In the case under consideration, the model predicts that an amount not exceeding 3.63 the initial mass of the thin disk was turned into stars during the earlier (A) stage of evolution.

## 6. CONCLUSION

The main results of the current paper may be summarized as follows.

- (1) The empirical differential oxygen abundance distribution (EDOD) inferred from two different samples for both the thin and the thick disk is consistent with a linear trend within four, three or two regions (Fig. 2).
- (2) A family of theoretical differential oxygen abundance distribution (TDOD) curves passing through the starting point  $(\phi_i, \psi_i)$  and the ending point  $(\phi_f, \psi_f)$  of the linear fit to

the EDOD is defined within the framework of simple multistage closed (box+reservoir) (MCBR) models. In addition, regions where the EDOD exhibits a linear trend are related to stages of evolution characterized by different inflow or outflow rate and/or different oxygen abundance within the flowing gas. The extreme curves of the family in the  $(O\phi\psi)$  plane are related to  $\zeta_O = 0, (\zeta_O)_\infty$ , the last corresponding to  $\kappa \rightarrow -\infty$ , for inflowing gas and  $\zeta_O = (\zeta_O)_\infty, A_O/(Z_O)_f$ , the first corresponding to  $\kappa \rightarrow +\infty$ , for outflowing gas.

- (3) For a family of TDOD curves corresponding to an assigned stage of evolution, all the parameters show a monotonic trend passing from the lower to the upper curve with the exception of the fractional stellar mass at the end of evolution which attains a maximum and, in consequence, cannot exceed a threshold. In particular, the model predicts that an amount not exceeding 3.63 the initial mass (Table 7) of the thin disk is turned into stars during the earlier (A) stage of evolution, in connection with the EDOD inferred from the PM11n sample.
- (4) The special case of steady inflow regime, where the TDOD reduces to a horizontal line, is consistent with the results of hydrodynamical simulations, where quasi equilibrium is attained between inflowing gas, outflowing gas and gas lost via star formation (e.g. Finlator and Davé 2008, Davé et al. 2011a,b, 2012).
- (5) If the linear trend inferred for the EDOD extends towards undetected low and high oxygen abundance, then the fractional star mass change does not exceed about 10% for well populated samples (PM11n, Ra11n, Ra11k) and about 20% for poorly populated samples (PM11k).
- (6) Under the assumption of a thick disk - thin disk collapse, model predictions yield a mass ratio  $M_K/M_N = 0.08, 1.89$  with regard to PM11 and Ra07 samples, respectively. The latter alternative is in contradiction with current observations, which seem to exclude the presence of a massive thick disk while the former remains available in this respect. If thick disk and thin disk stars belong to a single population (e.g. Bovy et al. 2012), no prediction can be made for or against a thick disk - thin disk collapse and the TDOD is expected to be slightly different from its counterpart related to the thin disk (Caimmi and Milanese 2009).

The main uncertainties on the EDOD used in the current paper are related to (i) poorly populated samples (PM11k); (ii) biased samples (all) towards low metallicities,  $[\text{Fe}/\text{H}] < -1.0$  or  $[\text{O}/\text{H}] < -0.5$ , which are expected to affect mainly the thick disk where the overall metallicity or oxygen abundance are lower than in the thin disk even if the low-metallicity tail is neglected. On the other hand, the prediction of early strong inflow implies the main features of thick and thin disk evolution are captured by the EDOD inferred from PM11n, Ra07n, Ra07k samples even if the low-metallicity tail is neglected.

*Acknowledgements* – Thanks are due to the referee S. Ninković for useful comments.

## REFERENCES

- Bovy, J., Rix, H.-W., Hogg, D. W.: 2012, *Astrophys. J.*, **751**, 131.
- Caimmi, R.: 2000, *Astron. Nachr.*, **321**, 323.
- Caimmi, R.: 2001a, *Astron. Nachr.*, **322**, 65.
- Caimmi, R.: 2001b, *Astron. Nachr.*, **322**, 241.
- Caimmi, R.: 2007, *New Astron.*, **12**, 289.
- Caimmi, R.: 2008, *New Astron.*, **13**, 314.
- Caimmi, R.: 2011a, *Serb. Astron. J.*, **183**, 37. (C11).
- Caimmi, R.: 2011b, *New Astron.*, **16**, 337.
- Caimmi, R., Milanese, E.: 2009, *Astrophys. Space Sci.*, **323**, 147.
- Davé, R., Finlator, K., Oppenheimer, B. D.: 2011a, *Mon. Not. R. Astron. Soc.*, **415**, 11.
- Davé, R., Finlator, K., Oppenheimer, B. D.: 2011b, *Mon. Not. R. Astron. Soc.*, **416**, 1354.
- Davé, R., Finlator, K., Oppenheimer, B. D.: 2012, *Mon. Not. R. Astron. Soc.*, **421**, 98.
- Fabbian, D., Nissen, P. E., Asplund, M., Pettini, M., Akerman, C.: 2009, *Astron. Astrophys.*, **500**, 1143.
- Finlator, K., Davé, R.: 2008, *Mon. Not. R. Astron. Soc.*, **385**, 2181.
- Fuhrmann, K.: 2008, *Mon. Not. R. Astron. Soc.*, **384**, 173.
- Holmberg, J., Nordström, B., Andersen, J.: 2007, *Astron. Astrophys.*, **475**, 519.
- Ibata, R. A., Gilmore, G. F.: 1995, *Mon. Not. R. Astron. Soc.*, **275**, 605.
- Ivezic, Z., Sesar, B., Juric, M. et al.: 2008, *Astrophys. J.*, **684**, 287.
- Malinie, G., Hartmann, D. H., Clayton, D. D., Mathews, G. J.: 1993, *Astrophys. J.*, **413**, 633.
- Norris, J. E.: 1987, *Astrophys. J.*, **314**, 175.
- Pagel, B. E. J.: 1989, *The G-dwarf Problem and Radio-active Cosmochronology*. In: Beckman J.E., Pagel B.E.J. (eds.) *Evolutionary Phenomena in Galaxies*, p.201. Cambridge University Press, Cambridge.
- Petigura, E. A., Marcy, G. W.: 2011, *Astrophys. J.*, **735**, 41.
- Ramirez, I., Allende Prieto, C., Lambert, D. L.: 2007, *Astron. Astrophys.*, **465**, 271.
- Rocha-Pinto, H. J., Maciel, W. J.: 1996, *Mon. Not. R. Astron. Soc.*, **279**, 447.
- Ryan, S. G., Norris, J. E.: 1991, *Astron. J.*, **101**, 1865.
- Wyse, R. F. G., Gilmore, G.: 1992, *Astron. J.*, **104**, 144.

**ЈЕДНОСТАВНИ МСВР МОДЕЛИ ХЕМИЈСКЕ ЕВОЛУЦИЈЕ:  
ПРИМЕНА НА ТАНКИ И ДЕБЕЛИ ДИСК**

**R. Caimmi**

*Dipartimento di Fisica e Astronomia, Università di Padova  
Vicolo Osservatorio 3/2, I-35122 Padova, Italy*

E-mail: roberto.caimmi@unipd.it

УДК 524.6–54 : 524.3–52–54

*Оригинални научни рад*

Једноставни вишефазни модели хемијске еволуције – затворена кутија + резервоар (тзв. МСВР модели), уведени у ранијим радовима, проширени су на случај доминантног прилива или одлива гаса у односу на гас заробљен у дугоживећим звездама и звезданим остацима. За задату емпиријску диференцијалну расподелу заступљености кисеоника, која се може апроксимирати линеарним фитом, направљена је фамилија кривих теоријских диференцијалних расподела заступљености кисеоника у складу са следећим предусловима: (i) почетна и крајња тачка линеарног фита су заједничке за све криве, (ii) параметар тока,  $\kappa$ , узима вредности од тачке екстремума до  $\mp\infty$ , где негативна и позитивна вредност за  $\kappa$  одговарају приливу и одливу, респективно, (iii) параметар одсецања,  $\zeta_0$ , узима вредности од тачке екстремума (која не може бити негативна) до граничне вредности,  $(\zeta_0)_\infty$ , повезане са  $|\kappa| \rightarrow +\infty$ . За криве са растућим  $\zeta_0$ , нађено је да удео масе гаса заробљеног у дугоживећим звездама и остацима има максимум да би затим пао на нулу при  $|\kappa| \rightarrow +\infty$ , док остали параметри имају монотони тренд. Приказана је и теоријска интегрална расподела заступ-

љености кисеоника. Резултати су примењени на емпиријску диференцијалну расподелу заступљености кисеоника добијену на основу два узорка звезда диска, за танки и дебели диск. У светлу овог модела размотрена су и ограничења везана за формирање и еволуцију. Еволуција је подељена на четири фазе: прикупљање (A), формирање (F), сажимање (C), равнотежа (E). Емпиријска диференцијална расподела кисеника за сваку од фаза слаже се са кривама за  $0 \leq \zeta_0 \leq (\zeta_0)_\infty$  у случају прилива гаса и за  $(\zeta_0)_\infty \leq \zeta_0 \leq 1.2$  у случају одлива гаса, са изузетком фазе A код танког диска где је област подударана ограничена на  $0.35 \leq \zeta_0 \leq (\zeta_0)_\infty$ . Фаза F се може описати као стационарни прилив ( $\kappa = -1$ ), што имплицира равну теоријску диференцијалну расподелу, што је у складу са резултатима хидродинамичких симулација. На крају, размотрена је (1) промена удела масе због екстраполације линеарног фита емпиријске диференцијалне расподеле на (недетектовани) реп мале металичности и реп високе металичности и (2) идеја ”колапса дебели диск – танки диск”, у светлу датог модела.